

## Chapter 4

### REPRODUCIBILITY OF SINGLE-PHOTON RESPONSES REFLECTS TIGHTLY CONTROLLED GPCR ACTIVITY

#### 4.1 Summary

The rod phototransduction cascade underlies sensitive visually guided behavior by encoding the arrival of single photons and their activation of individual molecules of rhodopsin, a G protein coupled receptor. A G protein-mediated cascade then amplifies receptor activity, resulting in remarkably reproducible fluctuations in rod outer-segment current, offering an elegant system to study and quantify mechanisms that transduce signals originating from single GCPGs. Here, we offer a rationale for a simplified model of stochastic receptor activity and transduction cascade, and we present an approach for evaluating how well the model, for a given set of parameter values, can account for measured properties of ensembles of isolated single-photon responses. We find that the model is well-constrained by experimental data, and that the constraints suggest that the transduction cascade responds linearly to receptor activity, and thus that response reproducibility reflects tightly controlled receptor activity.

#### 4.2 Introduction

Visually-guided behavior of vertebrates in near-darkness requires rod photoreceptors to detect and signal the arrival of single photons reliably (Field et al., 2005). The response to single photons is accomplished by amplifying the activity of a single molecule of rhodopsin, a G protein coupled receptor (GPCR), leading to a brief, detectable reduction in the current into the rod outer segment . This process provides an unparalleled opportunity to study how signals originating from single G-protein coupled receptors (GCPGs) are controlled

(Arshavsky et al., 2002). Though the unitary response reflects the activity of a single active rhodopsin, the resulting electrical responses have long been known to show much less variability in either amplitude or kinetics than might be expected (Baylor et al., 1979b).

The initial transduction steps are confined to the surface of membrane discs in the rod outer segment: rhodopsin catalytically activates the G-protein transducin, which in turn activates a cGMP phosphodiesterase, PDE6 (Wensel, 2008). Phosphodiesterase then hydrolyzes cGMP, perturbing its cytosolic concentration and causing cGMP-gated channels in the outer segment membrane to close, thus coupling the activity on the disc to the plasma membrane current. Rhodopsin activity shuts off through canonical GPCR desensitization reactions of phosphorylation and arrestin binding, PDE hydrolysis slows with transducin GTPase activity, and the current response recovers as cGMP is resynthesized by guanylyl cyclase (reviewed by (Arshavsky et al., 2002)). Calcium feedback to the guanylyl cyclase contributes to speed response recovery kinetics (Burns et al., 2002).

As a system, this signaling scheme produces responses that show much less variability than the typical first-order kinetics of other single-molecule processes, such as the charge flowing through an ion channel during a single opening. This reproducibility could, in principle, be explained either by low variability in the number of transducin molecules activated during the receptor lifetime or by nonlinearities in the transduction process that reduce the impact of higher variation in transducin activation. That is, the more variable the number of transducins activated, the stronger the nonlinear mechanisms would have to be to explain the reproducible nature of responses to single photons. Here, we develop a simple model to explore the trade-offs between sources of variability and mechanisms capable of suppressing this variability.

### 4.3 Methods

#### 4.3.1 Suction-electrode recordings

Suction electrode recordings of mouse rods were made as described, and single-photon responses were isolated based on their amplitude. Data used here to constrain models have been previously reported, with the exception of single-photon responses from *GCAP*<sup>-/-</sup> and *Rho*<sup>+//-</sup>/Tg(Rho/S388)lines (Azevedo and Rieke, 2011; Doan et al., 2006; Doan et al., 2009). For measuring features of ensemble variance across cells within a given line, responses are normalized to the peak amplitude of the cell average, and response time course is normalized to the time-to-peak.

We seek to identify likely characteristics of receptor kinetics and transduction that explain response properties across different mouse strains. If no genetic manipulations are made to change the cascade, a model should be able to account for response properties in lines with mutations that only affect receptor activity in well-described ways. To this end, we use responses from *GRK1*<sup>+//-</sup>, Tg(Rho/0P), and Tg(Rho/S388)/*Rho*<sup>-/-</sup> rods (Chen et al., 1999; Mendez et al., 2000; Doan et al., 2009; Doan et al., 2006). To control for effects of transgenic expression rhodopsin mutants, we also crossed *WT* and Tg(Rho/S388)/*Rho*<sup>-/-</sup> lines, and recorded from *Rho*<sup>+//-</sup>/Tg(Rho/S388) rods that express both normal and mutated rhodopsin.

Likewise, an accurate model of receptor activity will account for responses in rods with mutations that do not affect rhodopsin kinetics. Knockout of guanylyl cyclase accelerating protein (GCAP) removes calcium sensitivity of the cyclase and results in prolonged responses with larger amplitudes than *WT* rods, but should not affect activity on the disk. Likely parameters are those that can account for ensemble statistics in both *GCAP*<sup>-/-</sup> and *WT* rods simultaneously.

#### 4.3.2 Models

Below, we define parameters that govern a reduced model of the phototransduction cascade. We constrain the model to reflect the average properties of single-photon response ensembles, and evaluate parameters for their ability to replicate the properties of trial-to-trial variation in experimental data. Specifically, likely models will simulate responses with the following features (Fig. 4.1). First, the overall variability is low; the coefficient of variation of response area,  $CV_{area}$ , calculated as the standard deviation of response area divided by the mean, is in the range of  $\sim 0.3\text{-}0.35$  for normal mouse rods at  $37^{\circ}\text{C}$ , indicating that the reduction in charge influx varies by only  $\sim 35\%$ . Secondly, responses are less variable during the rising phase than during the falling phase, such that the response variance peaks later than the mean. The ratio of the time-to-peak of the variance to the time-to-peak of the mean for *WT* mice is around  $\sim 1.8$ . The variance also has a characteristic width,  $w_{\sigma^2}$ , measured at half height. One can think of these features as analogous to minimal parameters of other functions: a height ( $CV_{area}$ ), a width ( $w_{\sigma^2}$ ), and an offset ( $t_{peak,\sigma^2}/t_{peak,m}$ ).

In this study, we avoid detailed mechanistic descriptions in the service of exploring a few key parameters hypothesized to control properties of the response - simplifications which we justify below. Though intended to represent the effects of known mechanisms, we maintain a level of abstraction meant to schematize the cascade components.

#### *Stochastic model for rhodopsin activity*

We model receptor inactivation as a series of multiple shutoff steps, such that rhodopsin lifetime is effectively a sum of several sequential random, first-order lifetimes. The model receptor activity is specified by the number of shutoff steps, the reduction of activity produced by each inactivation step; and by the time scale of inactivation. Rhodopsin activity could alternatively be controlled by feedback, but studies have shown that  $\text{Ca}^{2+}$ -mediated

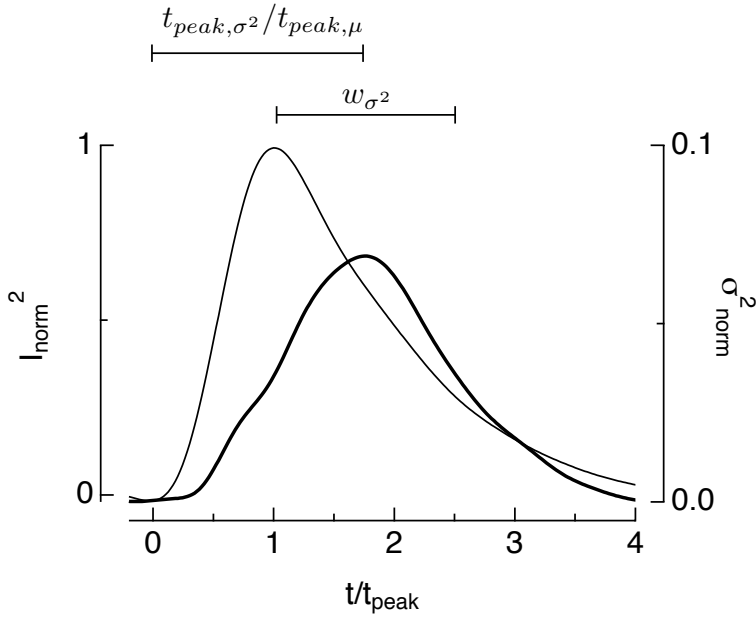


**Figure 4.1** – Features used in likelihood analysis. Data are from WT mice at 37°C. The normalized mean-squared response (thin trace, left axis) and single-photon response variance (thick trace, right axis) are plotted as a function of  $t/t_{\text{peak},\mu}$ , normalized to  $t_{\text{peak},\mu}$ , the time-to-peak of the mean.

feedback to rhodopsin is minimal during the single-photon response (Burns et al., 2002; Makino et al., 2004; Sampath et al., 2005; Chen et al., 2010), and we chose not to include it in our model.

Rhodopsin catalytic activity is assumed to begin at time,  $t = 0$ , and proceeds through a series of  $N_s$  steps (Fig 4.2B). Each step entails a reduction in rhodopsin's activity, given by  $\Delta Rh_i$ . These steps were determined by dividing the interval  $[0,1]$  into geometric sections,  $\Delta Rh_i$ , where  $\Delta Rh_{i+1} = (\delta^i)\Delta Rh_i$ . The initial step,  $\Delta Rh_1$ , will be set to ensure that the sum of all steps equals one (Fig 4.2B). The final step inactivates the remaining activity. Steps make equal drops when  $\delta = 1$  and  $\Delta Rh_i = 1/N_s$ . This scheme for defining  $\Delta Rh_i$  was chosen in order to model a wide range of reductions in activity with a single parameter, producing both step-like activity with a single transition ( $\delta \gg 1$ ) and activity that quickly

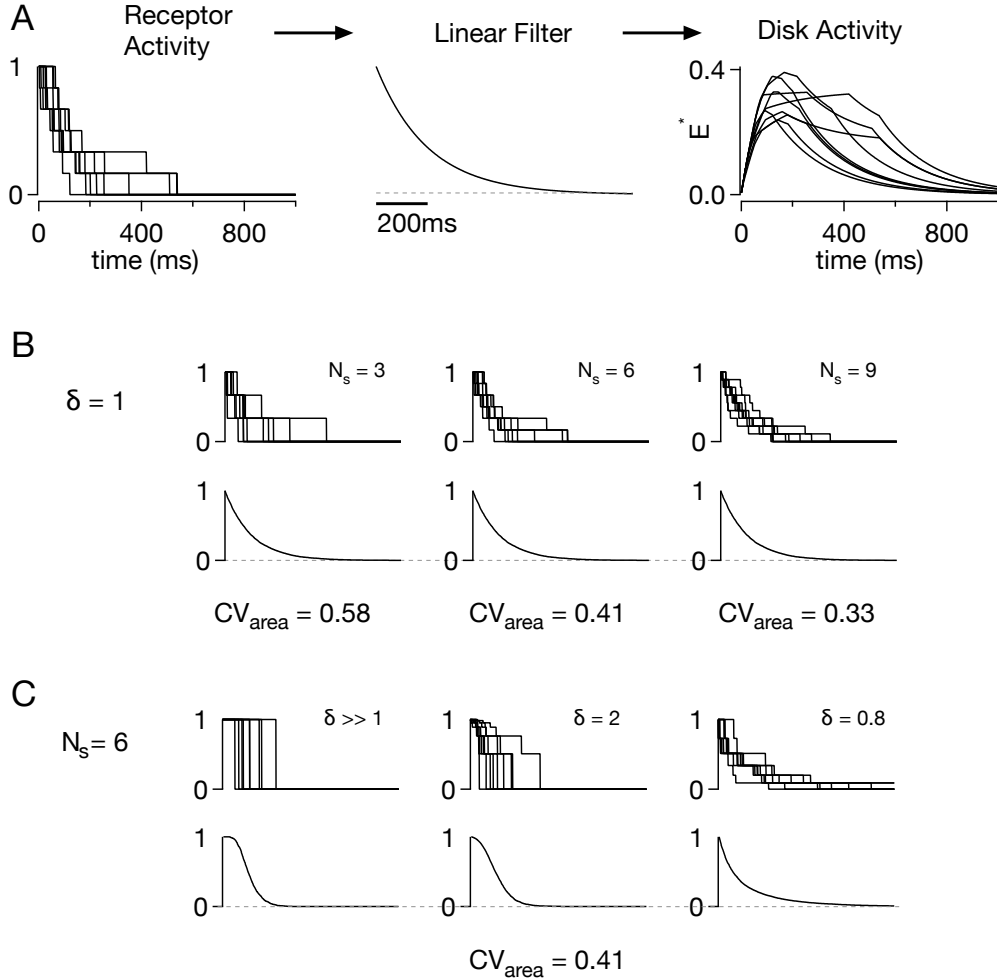


**Figure 4.2** – Parameters of stochastic receptor activity:  $N_s$ ,  $\delta$ ,  $T_{Rh}$ . A) Receptor activity simulated according to the model parameters (here:  $N_s = 6$ ,  $\delta = 1$ ,  $T_{Rh} = 150$  ms) gets convolved with a filter approximating the time scale of transducin inactivation (200 ms) to generate hydrolysis activity on the disk. The nine receptor trajectories generate the nine disk activity traces. Alternatively, PDE activity can also be stochastically generated as described in the text. B) The parameter,  $\delta = 1$ , is held constant as the number of steps in receptor shutoff increase. Nine traces in each panel. The average of  $N = 5000$  trajectories is unchanged with  $N_s$ , whereas  $CV_{area} \sim 1/\sqrt{N_s}$ . Time scale is arbitrary, set by  $T_{Rh}$ . C) The parameter,  $N_s = 6$ , is held constant as  $\delta$  decreases.  $CV_{area} = 1/\sqrt{N_s}$  is constant, but the shape of the average now depends on  $\delta$ .

is reduced, creating a long tail ( $\delta < 1$ ) (Fig 4.2C).

The average rate,  $k_i$ , at which rhodopsin takes the next step is then determined by

the activity level,  $Rh = 1 - \sum_i \Delta Rh_i$ , such that the ratio of rate and receptor activity is constant for all steps. At each point in time (here, sampled every millisecond), the next reduction in activity was made if a random number on interval  $[0, 1]$  was less than the rate per sampling period,  $\Delta T$ , for that step,  $k_i/\Delta T$ , a Bernoulli process. This scheme ensures that both the average and the variance of the activity (area) across steps are constant, providing a minimum in the variance of integrated activity across multiple steps (Hamer et al., 2005).

The total average activity is represented by  $T_{Rh}$ . The most general definition of  $T_{Rh}$  is the integral of the average receptor activity over time, and is given in units of time because receptor amplitude is scaled to a maximum value of one. This is a convenient definition when  $\delta = 1$  (the case when activity reduction is constant across steps) since the average response is a decaying exponential with time constant  $T_{Rh}$  (Fig. 4.2B). When  $\delta$  takes on different values, then  $T_{Rh}$  still represents the average activity (integral), but the balance of activity can shift towards late or early times (Fig. 4.2C)

### *Deterministic disk reactions*

In this study, we describe the set of reactions taking place on the disk simply as the effector activity, or disk activity,  $E^*(t)$ . We model the response of  $E^*(t)$  to an impulse of receptor activity as a deterministic, linear filter, described by an exponential decay (Fig 4.2A). Effector activity thus represents the time-course of both transducin and its target, PDE (Chen et al., 2000; Arshavsky and Bownds, 1992), as well as any delays between these reactions. The time course of this filter is well-constrained in the range  $\sim 200 - 250$  ms (Krispel et al., 2006). A deterministic response to receptor activity sets an upper bounds on variability introduced by rhodopsin. That is, if in reality steps other than rhodopsin introduce significant trial-to-trial fluctuations, then any bound we can put on reproducible

disk activity will mean even tighter control of rhodopsin desensitization. The result of this operation is a set of simulated trajectories of  $E^*(t)$ , as shown to the right in Figure 4.2A.

### *Compression of disk activity*

Nonlinearities within the transduction cascade could reduce the sensitivity of the measured currents to variability in rhodopsin or transducin activity. Such nonlinearities could take two general forms: (1) saturation of reactions on the membrane disc; (2) saturation of diffusible signals coupling disc activity to membrane channels. We can take several approaches to incorporating such saturation into stochastic models. The focus here is on simple empirical models that should encompass most forms of saturation.

The effector activity  $E^*(t)$  may not produce proportional changes in second messenger concentrations, as described below. Instead, as  $E^*(t)$  increases, for example, the effect of additional activity on the cascade may decrease. We model this reduced coupling as a Michaelis function, relating the effective activity on the disk,  $E(t)$ , to the effector time-course,  $E^*(t)$ :

$$E(t) = \frac{E^*(t)}{1 + K_E E^*(t)}. \quad (4.1)$$

where  $K_E$  has units of seconds and  $1/K_E$  in  $s^{-1}$  is the value of  $E^*(t)$  that compresses hydrolysis in half. This definition provides an intuitive connection between increasing values of  $K_E$  and increasing compression. Figure 4.3B depicts the effect of this type of nonlinearity, where the amplitude of  $E^*$  is compressed, and the average trajectory appears more rounded.

A second form of compression represents the effect of exhaustion without replacement of the available components on the disk, either transducin or PDE. Then the activity of  $E(t)$  is affected by the cumulative  $E^*(t)$ , and the more is activated, the less is available:

$$E(t) = \frac{E^*(t)}{1 + \kappa \int_0^t E^*(t') dt'}. \quad (4.2)$$

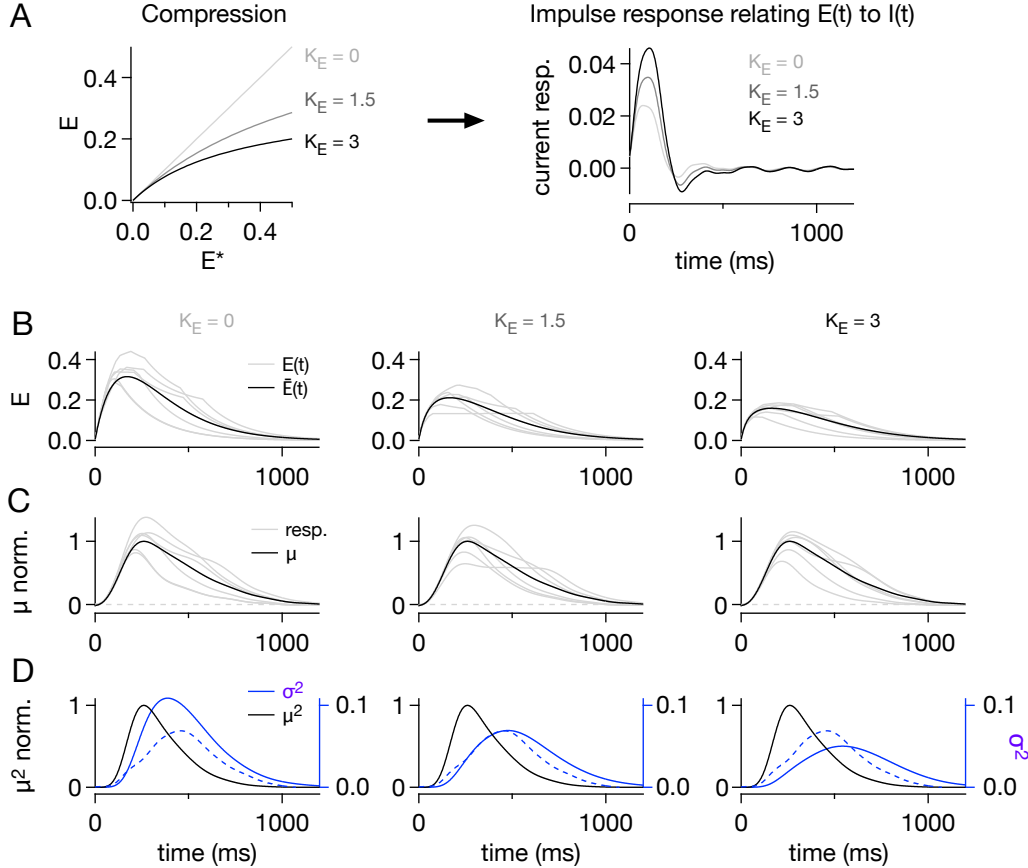


**Figure 4.3** – Compression of effector activity ( $K_E$ ), and subsequent linear filtering. A) Disk activity simulated as in Figure 4.2 is then passed through a compressing nonlinearity (left, Eq. 4.1). Trajectories are then filtered with an impulse response. B) Simulated  $E(t)$  trajectories with  $N_s = 6$ ,  $T_{Rh} = 150$  ms,  $\delta = 1$ . Larger values for  $K_E$  compress responses, changing the shape of the average disk activity,  $\bar{E}(t)$  (black traces). C) Effector activity is filtered by the impulse response in (A) to produce a set of output responses (grey traces), with an average response  $\mu(t)$  (black traces). The impulse response in (A) is calculated such that  $\mu(t)$  replicates the experimentally measured single-photon response. D) Ensemble time-dependent variance is unconstrained and depends on the model (blue traces, right axes). Note that variance is plotted on axes ten-fold smaller than the mean-squared activity (black trace, left axes). Experimentally-measured variance (Fig. 4.1), is replotted in each panel for reference (blue dotted traces).

The effect of this type of nonlinearity is to compresses both the amplitude and time course of  $E^*(t)$ , as shown in Figure 4.4

The output of the nonlinear relationships, the compressed trajectories,  $E(t)$ , represent

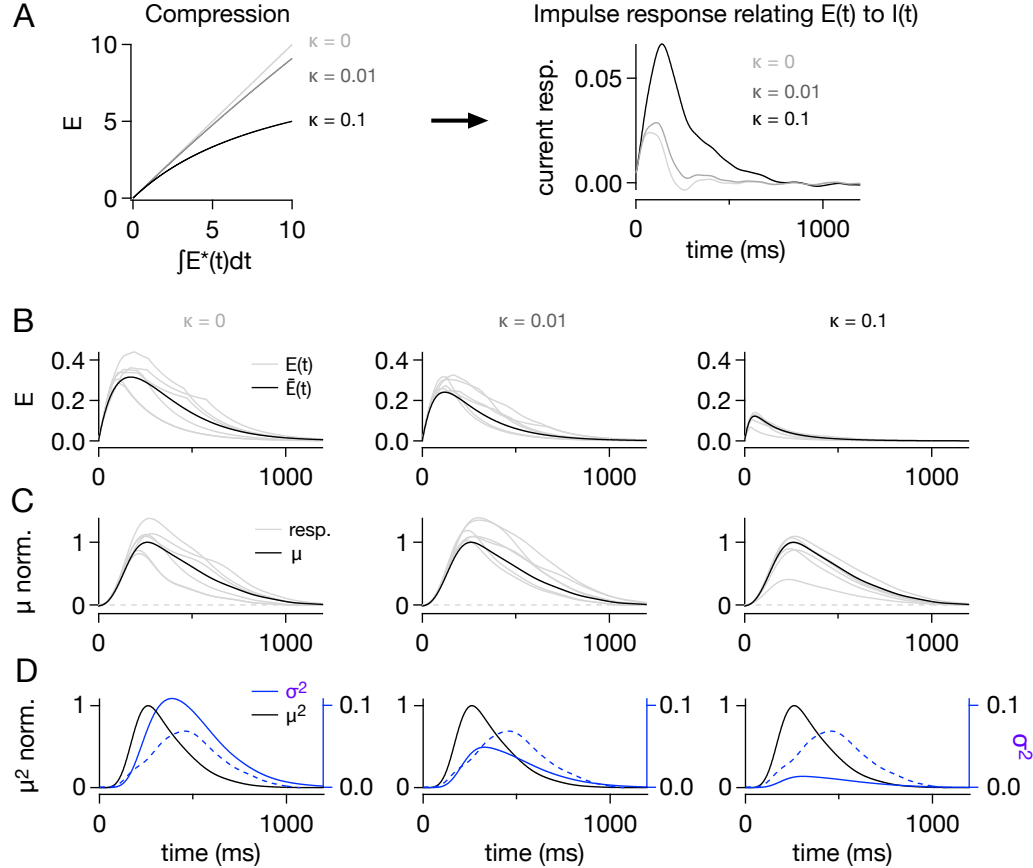


**Figure 4.4** – Saturation of effector activity ( $\kappa$ ), and subsequent linear filtering. A) Disk activity simulated as in Figure 4.2 is then passed through a nonlinear saturation function that depends on the integrated  $E^*(t)$  activity (left, Eq. 4.2). Trajectories are then filtered with an impulse response. B) Simulated  $E(t)$  trajectories with  $N_s = 6$ ,  $T_{Rh} = 150$  ms,  $\delta = 1$ . Larger values for  $\kappa$  compress responses, changing the shape of the average disk activity,  $\bar{E}(t)$  (black traces). C) Effector activity is filtered by the impulse response in (A) to produce a set of output responses (grey traces), with an average response  $\mu(t)$  (black traces). The impulse response in (A) is calculated such that  $\mu(t)$  replicates the experimentally measured single-photon response. D) Ensemble time-dependent variance is unconstrained and depends on the model (blue traces, right axes). Note that variance is plotted on axes ten-fold smaller than the mean-squared activity (black trace, left axes). Experimentally-measured variance (Fig. 4.1), is replotted in each panel for reference (blue dotted traces).

the time-course of changes in second messenger concentration that will then determine the current response. These trajectories incorporate all of the intervening reactions between receptor and second messenger, including any delays or saturation of components.

*Linear model relating current to changes in second messenger concentration.*

Thus far, a specific stochastically generated trajectory for receptor activity is passed through a linear filter representing disk activity, then acted on by compressive nonlinearities to generate fluctuations of second messenger,  $E(t)$ . For each set of parameters, we simulate  $> 5000$  such trajectories, and average to produce a mean trajectory,  $\bar{E}(t)$  (Fig. 4.3B and Fig. 4.4B, black traces).

To then transform disk activity trajectories into current responses (Fig. 4.3C and Fig. 4.4C, grey traces), we calculate an empirical, deterministic response function which incorporates the remaining elements of the transduction cascade (Fig. 4.3A and Fig. 4.4A). Here, we consider only a linear cascade, where additional  $E$  activity proportionally perturbs the current, a picture we justify below. We constrain the transduction impulse response,  $F$ , to match the measured single-photon response, given the average second messenger trajectory,  $\bar{E}(t)$ , with Fourier transform  $\tilde{E}(\omega)$ . To do so we calculate  $F$  as a filter with a Fourier transform given by

$$\tilde{F}(\omega) = \frac{\tilde{I}(\omega)}{\tilde{E}(\omega)}, \quad (4.3)$$

where  $\tilde{I}(\omega)$  is the Fourier transform of the measured single-photon response. In this way, each trajectory,  $E(t)$ , is filtered by  $F$  to generate an ensemble of  $> 5000$  current responses, and the average of the ensemble exactly matches the experimental average single-photon response (Fig. 4.3C and Fig. 4.4C, black traces).

#### 4.3.3 Evaluating model performance

While the procedure for choosing  $F$  above guarantees a perfect match between the simulated ensemble mean and the average measured single-photon response, the ensemble variance is not similarly constrained and instead reflects the properties of the underlying model (Fig. 4.3D and Fig. 4.4D, blue traces). We evaluated each model based on how well it

captured experimentally-defined features of the single-photon response variations.

For each cell, we measured a set of features,  $x_i$ , a term we use to differentiate between parameters of the model and parameterization of ensemble variance, illustrated in Figure 4.1. Empirically we found that a combination of the coefficient of variation of the response area (the ratio of standard deviation to the mean,  $\text{CV}_{\text{area}}$ ), the time-to-peak of the variance relative to the mean ( $t_{\text{peak},\sigma^2}/t_{\text{peak},\mu}$ ), and the width of the variance ( $w_{\sigma^2}$ ) provided good separation among models. These features of single-photon response have been reported previously and some have been used to constrain models in the past (Field and Rieke, 2002a; Rieke and Baylor, 1998a). Experimental samples are then the set of all features in each cell,  $\mathbf{x}_k = \{x_i\}_k = \{\text{CV}_{\text{area}}, t_{\text{peak},\sigma^2}/t_{\text{peak},\mu}, w_{\sigma^2}\}_k$ . We make the further assumption that features are uncorrelated, for example that  $\text{CV}_{\text{area}}$  does not increase with  $w_{\sigma^2}$  and that we can evaluate each feature independently. In order to minimize variation in feature values due to differences across cells, we normalize responses from each cell by the amplitude and time-to-peak of the cell's averaged response. The optimal model will provide as close a match to the measured features,  $\{\hat{x}_i\}$ , as possible.

For parameters  $\theta$ , we simulated responses and extracted the values of the ensemble variance features,  $\{\mu_i\}$ . Enough responses were simulated to eliminate variability in feature values across multiple simulations. Then, we calculate the probability that the feature,  $\mu_i$ , has a value between  $\mu_i$  and  $\mu_i + d\mu_i$ :

$$p(\mu_i|\theta) = \frac{1}{\sqrt{2\pi\sigma_i^2}} \exp\left(-\frac{-(\hat{x}_i - \mu_i)^2}{2\sigma_i^2}\right). \quad (4.4)$$

where  $\sigma_i$  is the standard error of the mean  $\hat{x}_i$ . By using this formulation, we are assuming that the sample mean,  $\hat{x}_i$ , reflects the true feature value with some error. This error could be due to finite sampling effects, since, because we could only measure  $\sim 50 - 100$  single-photon responses per cell retained for analysis, we can only estimate the true ensemble variance for that cell. In the model, on the other hand, we can simulate enough responses such

that features have negligible error from one trial to the next. Then, the above definition is equivalent to the probability of observing a sample mean  $\hat{x}_i$  if we were measure  $N$  cells and if the true value for a feature is  $\mu_i$ .

We then define the function  $l(\theta)$  for a given set of parameters as

$$l(\theta) = \prod_i p(\mu_i|\theta). \quad (4.5)$$

In other words,  $l(\theta)$  is the product across features of the probability of observing an average feature value  $\hat{x}_i$  with SEM  $\sigma_i$  if the true value of the feature is  $\mu_i$ . This provides a measure of how well a given model captured key features of the experimental responses. The best parameters are those which produce the smallest difference between simulated and experimental variance and maximize  $l(\theta)$ , where a perfect agreement is given by  $d(0|\theta)$

This approach is analogous in some ways to a maximum-likelihood calculation, where typically the likelihood of observing the experimental samples  $\mathbf{x}_k$ , given  $\theta$ , is

$$L(\theta) \equiv p(\mathcal{D}|\theta) = \prod_k p(\mathbf{x}_k|\theta), \quad (4.6)$$

where  $\mathcal{D}$  is the set of independent experimental samples and  $p(\mathcal{D}|\theta)$  is the probability of observing those samples. Often, a model may be an analytical and well-defined function of  $\theta$  that would permit optimizing the likelihood function through gradient descent. This approach would also necessitate estimating the conditional distributions  $p(\mathbf{x}_k|\theta)$ . Here, though, the parameters establish a set of stochastic processes, with no clear analytical relationship to the output features, and we instead take the approach of numerically exploring parameter space and assuming the mean feature value is an appropriate target.

#### 4.4 Results

Variability in single-photon responses has been characterized in rods from several species (Rieke and Baylor, 1998a; Whitlock and Lamb, 1999; Field and Rieke, 2002a; Doan et

al., 2006). The trial-to-trial fluctuations share a number of common features, illustrated in Figure 4.1, specifically, low overall variability ( $CV_{area} \sim 0.3$ ) and more variability late in the response than early, quantified by the ratio of time to peak of the ensemble variance relative to that of the mean response ( $t_{peak,\sigma^2}/t_{peak,m}$ ). How do interactions between elements of the cascade lead to these characteristics? In particular, where does variability arise and how is it mitigated? We first assess the extent to which the cascade acts linearly on rhodopsin activity, and establish a range of nonlinear models that can account for experimentally-measured responses. Thereafter, we explore parameter space for models that include nonlinear effects and ask how these parameters can trade-off to control the properties of the response variance.

#### *4.4.1 Experimental data constrain the strength of nonlinear mechanisms*

An important consideration is whether elements of the cascade are linear. Put plainly, do two active transducins produce, on average, twice the effect of one (linear), or does the second amplify (supra-linear) or compress (sub-linear) the effect of the first? Linearity could fail in two broad ways: (1) nonlinear interactions of the disc-associated reactions — e.g. depletion of available transducin or PDE; (2) nonlinearities associated with the post-disc reactions — e.g. depletion of cGMP or channels. This separation is important for interpretation of experiments aimed at testing linearity.

#### *Linear dependence of current on changes in cGMP*

Several lines of evidence suggest that the current responds linearly to changes in cGMP. Neither manipulation of  $\text{Ca}^{2+}$  feedback to guanylyl cyclase nor delivery of multiple photons to a local region of the outer segment reveal response nonlinearities (Burns et al., 2002; Field and Rieke, 2002a). These experiments suggests that over the range of reduction in cGMP that would result from activation of a single receptor, additional changes in cGMP have proportional effects on the current. Under these conditions, then, fluctuations in

cGMP are unlikely to strongly recruit nonlinear mechanisms such as local channel closure, or cooperative mechanisms in channel gating or  $\text{Ca}^{2+}$  feedback. This also provides a rationale for relating average disk activity to current responses using a linear impulse response (see section 4.3.2).

#### *Linearity of disk reactions*

While changes in current are linearly related to changes in cCMP, it is not clear whether additional activity on a given disk will hydrolyze proportionate amounts of cGMP. For example, hydrolysis depends both on the activity of PDE and on the local concentration of cGMP. As the local pool of cGMP within the disk space is hydrolyzed, additional PDE activity may be less effective (Bisegna et al., 2008). By testing manipulations of rhodopsin activity rather than downstream components of the cascade, we can test for both disc-associated and post-disc nonlinearities. Ideally, we would activate two rhodopsins on a disk and directly test whether the second active receptor affects the signal from the first, but this would require control of the spatial location of photon absorption to better than 50 nm.

Alternatively, we can ask whether genetic alterations that increase rhodopsin's activity reveal nonlinear mechanisms, as laid out below. Key to this approach is not only that we increase receptor activity but also that we can accurately quantify that increase. Thus, we compared single-photon responses in which phosphorylation had been slowed. Rods from (*GRK1<sup>+-</sup>*) exhibit prolonged single-photon responses relative to normal rods, which reflect a relatively slow rhodopsin decay time constant of 640 ms (Doan et al., 2009). Preventing phosphorylation altogether, through mutations to rhodopsin's C-terminus that remove all phosphorylation sites (0P), leads to severely prolonged, step-like responses, indicating receptor activity is also step-like, with little inactivation during the first  $\sim 1 - 2$  seconds of the response (Mendez et al., 2000). If we assume that the initial rates of G protein

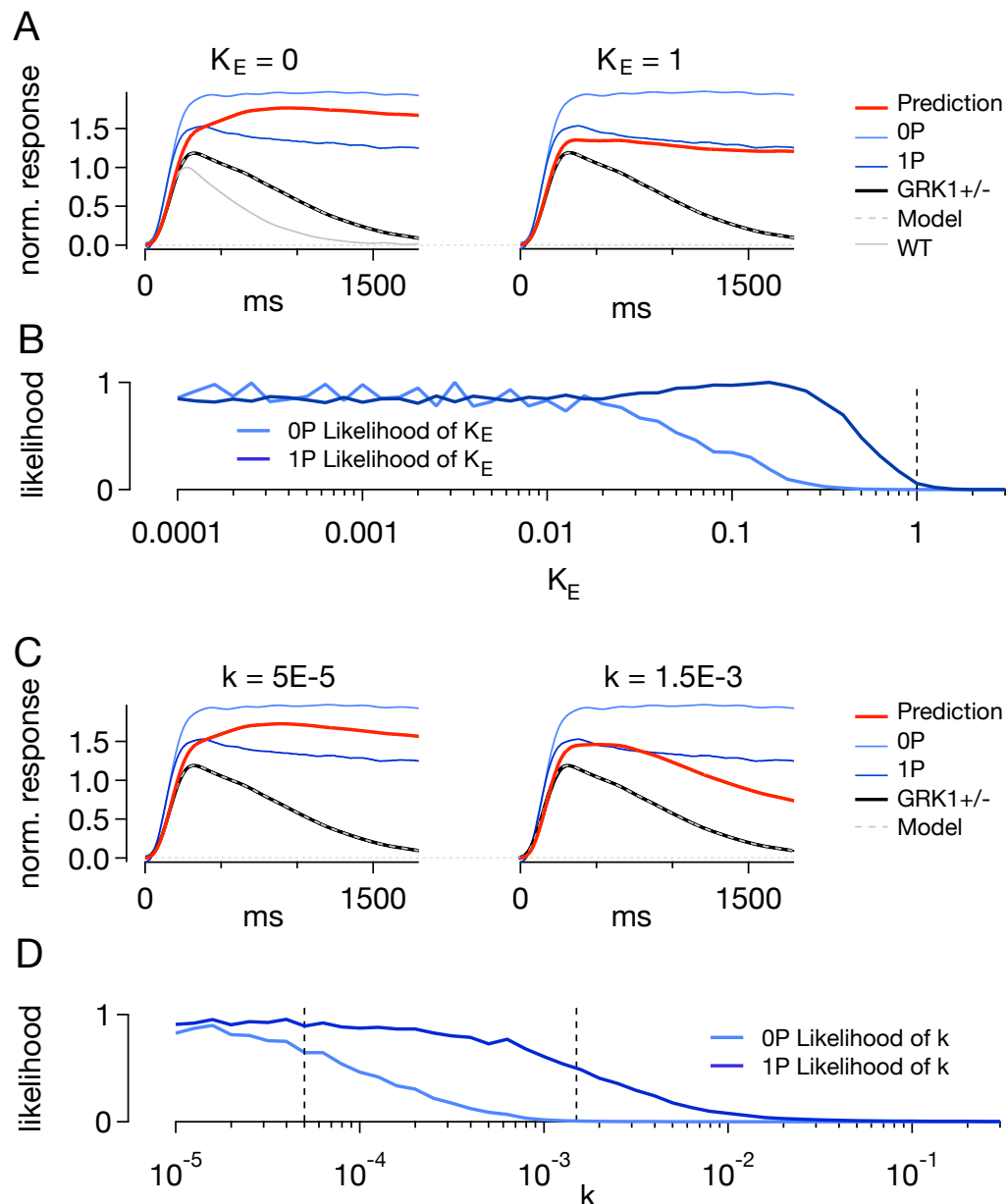
activation are equal, both mutations may be expected to engage any forms of saturation or compression on the disk more than in normal rods. If we include nonlinear effects, what parameter values for compression can account for the data from experiment?

We simulated  $GRK1^{+/-}$  receptor activity with  $T_{Rh} = 640$  ms,  $N_s = 8$ , and  $\delta = 1$ , and modeled disk reactions as a deterministic process with  $\tau_G = 200$  ms (Fig. 4.5). We varied forms of compression ( $K_E$ , and  $\kappa$ ) and calculated the average disk activity,  $\bar{E}(t)$ , as in Figure 4.3. We then calculated the impulse response function that provides a match to the average  $GRK1^{+/-}$  response. Both the experimental and the model average are shown in Figure 4.5A (model, grey dotted trace;  $GRK1^{+/-}$ , thick black trace), and are normalized to the average  $WT$  response (grey trace). The filter and compression were then held constant while we altered rhodopsin parameters to simulate the mutant 0P activity ( $T_{Rh} = 23.4$  s,  $N_s = 1$ ) (Doan et al., 2006).

Figure 4.5 compares the measured 0P responses (light blue) with those of  $GRK1^{+/-}$  rods (trace black trace). The mean single-photon response from normal rods is shown for comparison. The predictions of the model are shown with thick red traces. The predicted response without compressive effects is, if anything, slightly smaller than those measured (Fig. 4.5A, left,  $K_E = \kappa = 0$ ). Naturally, as compression increases, the amplitude of the model prediction decreases (Fig. 4.5A, right), and the likelihood also declines (Fig. 4.5B,D).

Mouse transgenesis can lead to varying amounts of protein expression (Nagy, 2003). For 0P and 1P rods, this can lead to random levels of rhodopsin expression, and may cause rods to compensate, possibly changing response kinetics (Liang et al., 2004). It was noted that 0P rods are shorter than  $WT$  rods, and it is possible that a decrease in length for 0P rods implies an accompanying decrease in plasma membrane surface (its width may also expand). Rods expressing 0P rhodopsin have normal dark currents, so if the cGMP concentration remains the same in a smaller rod, the increased amplitude of 0P responses

**Figure 4.5** – Likelihood estimates of nonlinear parameters using responses to step-like rhodopsin activity. Likelihood represents how well the predicted response (thick red lines) matches the amplitude of either 0P (light blue) or 1P (dark blue) responses. A, C) Average single-photon responses for all lines, normalized to *WT* response (0P - light blue; 1P - dark blue; *GRK1<sup>+/−</sup>* thick black; *WT* as reference - thin grey). The model provides perfect match between average simulated activity and *GRK1<sup>+/−</sup>* response (dotted grey over black). Thick red line shows response of the same model to a step of rhodopsin activity. Values for parameter shown above. B, D) Likelihood of observing measured response amplitude (0P - light blue; 1P - dark blue) as a function of saturation; B)  $K_E$  is varied while  $\kappa = 0$ , and D) vice versa. Black dotted lines indicate values depicted in (A) and (C).



may be due to a higher density of channels (Caruso et al., 2010). As a control for this effect, we measured responses from rods expressing both WT and S338 (1P) forms of rhodopsin (the 0P line is no longer available).

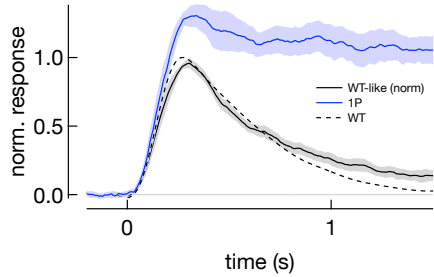


**Figure 4.6** – Responses in rods with 1P and WT rhodopsin co-expression at 30°C. Responses from S338 (1P) rhodopsin could be distinguished by their prolonged activity (blue trace,  $\pm$ SEM). Responses that are identified as originating from WT rhodopsin (black trace) show similar kinetics to responses recorded in rods of *WT* mice (dotted line).

Responses to 1P activation were easily identified by their prolonged activity. The resulting ensemble reached a larger amplitude on average than normal responses, similar to those reported in *Tg(Rho/S388)/Rho<sup>-/-</sup>* in our recording conditions (Doan et al., 2006). Figure 4.6 compares the results of these recordings with the average response in *WT* rods; the 1P response amplitudes are used in the analysis described below and in Figure 4.5A,C (dark blue lines). As previously observed, 1P response amplitudes are not as large as 0P responses, though still larger than in *GRK1<sup>+-</sup>* rods (Fig. 4.5). The reduction in amplitude was proposed to reflect fast phosphorylation of the single remaining site, reducing the rate of transducin activation (Gibson et al., 2000; Mendez et al., 2000).

Regardless, we assume rhodopsin activity is step-like as above ( $T_{Rh} = 18.8$  s,  $N_s = 1$ ) (Doan et al., 2006), and ask whether compression of the cascade can account for the difference in S338 vs. *GRK1<sup>+-</sup>* amplitudes, and if so, for what range of values is likelihood high?

Figure 4.5 plots the probability of observing the mean S338 amplitude (when expressed

along with normal rhodopsin) for a given set of parameters if the cascade is constrained to mimic the  $GRK1^{+/-}$ -responses. In this case, larger values of compression parameters become more likely, where eventually values of  $K_E > 1$  lead to model predictions  $> 50$ -fold less likely. In particular, values of  $\kappa$  appear to range further. However, the right panel in (C) shows that even for values that provide a good match to the amplitude, as more PDE is activated and used up, less is available and the response begins to recover. We conclude that this behavior makes this form of saturation unlikely and we focus below on the compression of disk activity (Eq. 4.1).

Thus far, in Figures 4.5 and 4.6, we have evaluated how well different models account for responses in mutants with prolonged receptor activity. In doing so, we have shown that a linear cascade provides a likely explanation for mutant responses, but that models with some compression ( $K_E < 1$ ) can also explain the data. However, in the following sections we use additional features of experimental data to show that values of  $K_E$  within the allowable range are unable to suppress variability in receptor activity. In order to present this evidence, we first develop our method of evaluating particular model parameters and then investigate how different parameters control the model's behavior.

#### 4.4.2 Constrained nonlinearities do not suppress variability in receptor activity

Could the variability due to stochastic receptor activity, at the input to the cascade, be suppressed by the effects of compression acting downstream, within the range established by experiments in Figure 4.5? To address this question, we asked how well a set of parameters captured the total response variability ( $CV_{area}$ ), the time-to-peak of the variance relative to the mean response ( $t_{peak,\sigma^2}/t_{peak,m}$ ), and the width of the variance ( $w_{\sigma^2}$ ) (see Fig. 4.1).

Figure 4.7 illustrates this approach for a linear cascade ( $N_s = 10$ ,  $T_{Rh} = 225$  ms,  $K_E = 0$  s) while varying the parameter  $\delta$ . We find that  $\delta \sim 1$ , in which case, average rhodopsin

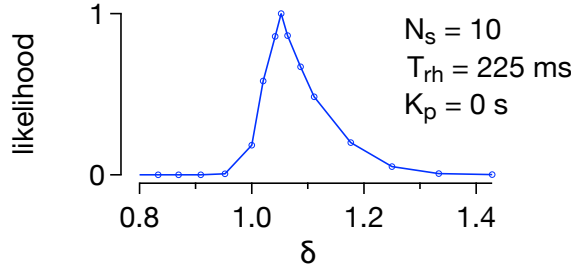


**Figure 4.7** – Likelihood profile across parameter values governing reduction in rhodopsin activity (WT at 36C). Other parameters were held fixed.

activity follows an exponential decay, with time constant  $T_{Rh}$ . We fix this parameter below to simplify the demonstration of model behavior as nonlinearities are included. We then generated responses across a range of receptor lifetimes  $25 \leq T_{Rh} \leq 325$  and shutoff steps,  $3 \leq N_s \leq 12$ , while also varying the compression of disk activity,  $0 \leq K_E \leq 5$ . Note, for illustration purposes, we have extended the range of compression beyond those suggested by the experiments of Figure 4.5.

Figure 4.8A plots contours of constant log-likelihood for values of compression,  $K_E$ , and receptor decay time constant,  $T_{Rh}$ , where the number of shutoff steps  $N_s$  is held constant in each panel (shown above each panel). The color scale is constant across panels, with red indicating likely parameters, and each contour line reflecting a  $10^{\frac{1}{4}}$  reduction in likelihood, such that the transition from green to blue reflects parameter values that are 100-fold less likely to represent the data, and violet indicates a factor of  $10^{-4}$ . Grey lines plot the maximum likelihood parameters for reference ( $N_s=7$ ,  $T_{Rh}=175$  ms, and  $K_E=2$ ), and as  $N_s$  changes, the most likely values of  $T_{Rh}$  and  $K_E$  can be seen to drift.

As we might naively expect, the likelihood landscapes show that nonlinear coupling of disk activity,  $E(t)$ , with the transduction filter can mitigate the effects of variability on the disk. First, as the number of steps decreases (leftward through panels), compression must

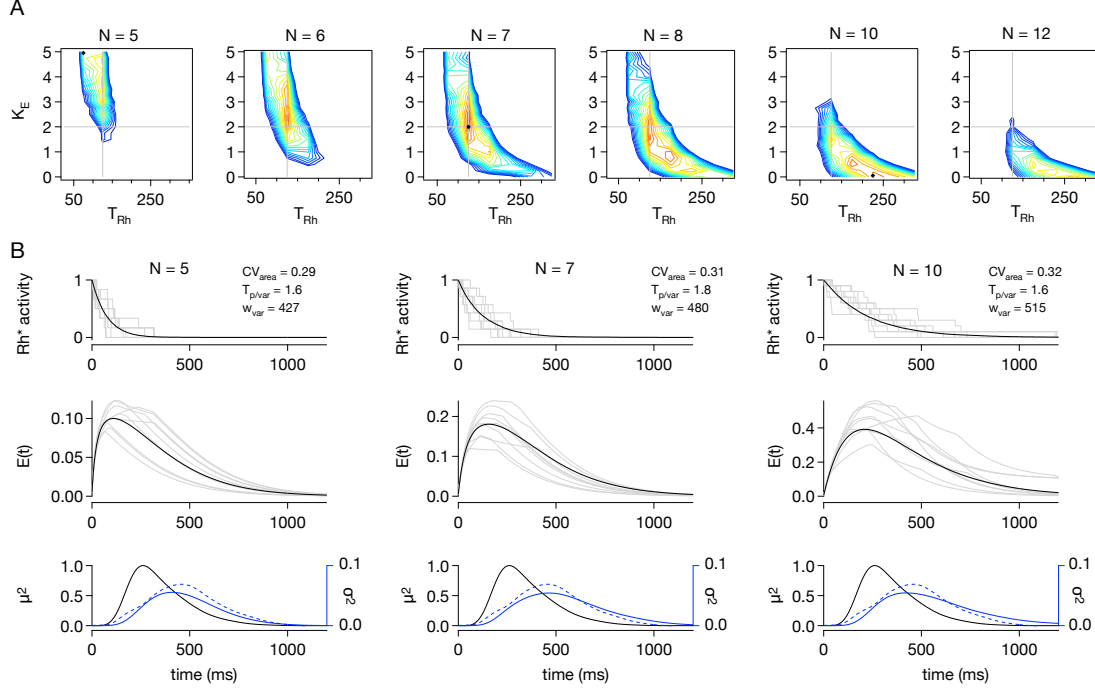


**Figure 4.8 – Likelihood landscapes across parameters,  $K_E$ ,  $T_{Rh}$ ,  $N_s$ , compared to WT at 36C.** A) Log-likelihood is plotted in contours (0.25 log units each), where green hues represent a reduction in likelihood of  $\sim 100$ . Grey lines plot maximum-likelihood estimates for the parameters  $K_E$  and  $T_{Rh}$ . B) Example models for parameters represented as black diamonds in panels in A. Example trajectories are shown in grey, averages of 5000 simulated trajectories in black. Note the different scales for  $E(t)$  as compression changes. Lower panels compare the model ensemble time-dependent variance (blue traces, right axes) with the experimentally measured variance (dotted blue traces, right axes). The two models on the left are not within the constraints of Figure 4.5.

increase to offset fewer steps (y-axis). At the same time, the time constant of receptor decay also decreases (x-axis), until when  $N_s \leq 7$ ,  $T_{Rh} \sim 125$  ms remains the most likely estimate. The traces below help to illustrate model behavior by showing intermediate trajectories at each stage for the parameters indicated by the crosses in the panels above. With few shutoff steps, substantial compression was required to reduce the variability to match experiment (Fig. 4.8B, left). This compression decreases variability near the peak of the PDE activity,

but not during the falling phase, hence pushing the variance to later times. To counter this effect and match the measured time-to-peak of the variance,  $T_{Rh}$  must be reduced. Conversely, a longer time constant ( $\sim 225$  ms) is required to account for this late variance when  $N_s$  increases and compression is relieved. These parameters trade smoothly and permit a large range of compressive effects: when  $N_s = 6$ , a value of  $K_E = 2.5$  is still highly likely.

Figure 4.9 depicts the same range of models evaluated for their ability to account for larger and slower single-photon responses in  $GCAP^{-/-}$  rods (at 37°C) which lack  $\text{Ca}^{2+}$  mediated acceleration of cGMP synthesis. We would expect a common stochastic model for rhodopsin inactivation to account for responses in both *WT* and  $GCAP^{-/-}$  rods as knock-out of GCAP proteins should not affect any of the mechanisms involved in G protein activation or receptor desensitization. In addition, experiments in which  $\text{Ca}^{2+}$  concentration in  $GCAP^{-/-}$  rods is buffered with BAPTA suggest that changes in  $\text{Ca}^{2+}$  have little affect on the single-photon response except via control of cGMP synthesis (Burns et al., 2002). If anything, we might expect that local cGMP concentration in the disk space would be replaced more slowly, thus exacerbating hydrolysis rate compression,  $K_E$ . This appears not to be the case; rather, we find generally the same trend as for *WT*, with higher values for suppression relatively less likely, but with consistent expectations for receptor kinetics.

Finally, we return to our initial question of whether nonlinearities permitted by the comparison between  $GRK1^{+/+}$  and 0P responses (Fig. 4.5) can offset variability introduced by stochastic receptor activity. Compression values  $K_E > 0.5$  failed to capture the amplitude of 0P and 1P responses. By reviewing the contour plots in Figures 4.8 and 4.8, we can see that if  $K_E$  is restricted to values within this range, then the data are best explained by rhodopsin inactivation requiring 8-11 steps with a  $T_{Rh}$  of 175 – 250 ms in both *WT* and  $GCAP^{-/-}$  rods. Over this range, then, compression is does not dramatically alter the characteristics of the single-photon response variance, implying that reproducibility of the

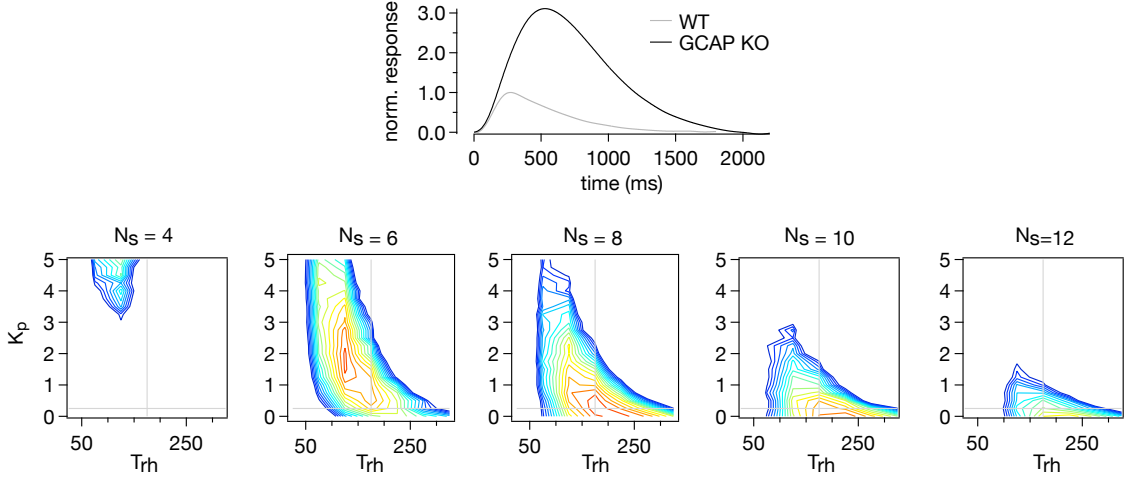


**Figure 4.9** – Likelihood landscapes across parameters,  $K_E$ ,  $T_{Rh}$ ,  $N_s$ , for models of  $GCAP^{-/-}$  responses at 37°C. A) Average single-photon responses of WT (grey) and  $GCAP^{-/-}$  (black) rods. Responses are normalized for comparison with Fig. 4.5. B) Log-likelihood is plotted in contours (0.25 log units each), where green hues thus represent a reduction in likelihood of  $\sim 100$ . Grey lines plot most likely values for the three parameters.

single-photon response directly reflects reproducible receptor activity.

#### *Consequences of a linear cascade*

A linear cascade allows an intuitive explanation for the dependence of likelihood on various parameters. For linear models,  $CV_{area}$  is controlled entirely by the number of inactivation steps and hence directly constrains this parameter. The  $t_{peak,\sigma^2}/t_{peak,m}$  depends primarily on the duration of rhodopsin's activity relative to the kinetics of the transduction cascade filter, with a weak dependence on the number of steps. Finally the width of the variance is primarily determined by how much activity declines following each step; with little decline following each step, the variability all occurs in a narrow window following the final decay step, whereas with a distribution of decay across steps, variability is more spread out over time.

### *Possible sources of variability*

We have chosen stochastic fluctuations in receptor activity to be the source of trial-to-trial variability in our model. In reality, the number of activated transducin or PDE molecules is also stochastic, which we have avoided including here. To see the implication of this choice consider a linear cascade process, such that additional activity at any point in the cascade causes a proportional change in the current. Regardless of its kinetic properties, a linear cascade does not change the coefficient of variation of the single-photon response area. If rhodopsin is the sole source of variability, then coefficient of variation of the current area is identical to the coefficient of variation of rhodopsin's integrated or cumulative activity. Intuitively, this equality originates because the relation between the area of a given rhodopsin trajectory and the current is given by the area of the linear transduction filter — i.e. a single scalar number. This scale factor affects the mean and standard deviation of the responses equally and will not change the coefficient of variation. The  $\text{CV}_{\text{area}}$  is then an upper bound on trial-to-trial variation in rhodopsin activity, and if we were to model transducin activity as stochastic, rhodopsin inactivation would have to be even more tightly controlled to produce the low  $\text{CV}_{\text{area}}$  that we observe experimentally. Thus, in the simple multi-step shutoff model here, rhodopsin inactivation would require a minimum of 8 to 11 steps to explain the measured  $\text{CV}_{\text{area}}$  of 0.3 to 0.35 (i.e.  $\text{CV}_{\text{area}} = 1/\sqrt{N_s}$ ).

### **4.5 Discussion**

Rod phototransduction presents a unique opportunity to explore enzyme cascades and GPCR mediated signaling quantitatively. Here, we use the characteristics of ensembles of isolated single-photon responses to explore the behavior of a simple model for coupling the activity of the GPCR rhodopsin to the rod outer-segment current, and compare across normal mice and a number of transgenic lines. Our results show that explaining response

properties across a number of genetic lines requires a cascade that effectively acts linearly on the receptor throughout its active lifetime. Consequently, the low variability of the single-photon response provides an upper bound on variability in receptor activity and thus implies tight regulation of the total receptor activity. Spreading total activity across multiple steps, each with first order kinetics, provides an efficient description of a process with low intrinsic variability, and in this context, rhodopsin desensitization requires at least 8 steps and a time constant of  $\sim 225$  ms.

#### *4.5.1 Multi-step models of rhodopsin desensitization*

The low variability of single-photon response ensembles has provided a valuable target for models of phototransduction reaction dynamics, and as such these higher order characteristics have inspired efforts to identify their origin, first in amphibian rods (Rieke and Baylor, 1998a; Whitlock and Lamb, 1999; Hamer et al., 2003; Hamer et al., 2005) and subsequently in mammalian rods (Mendez et al., 2000; Field and Rieke, 2002a; Doan et al., 2006; Doan et al., 2009). Experiments and modeling in amphibian rods suggest that rhodopsin desensitization is tightly regulated to introduce low variability in the number of active transducin molecules across responses. Molecular properties are not as well measured in mammalian rods, prompting the use of signatures of the time-dependent variance to constrain models, the approach adopted here for mouse rods (Field and Rieke, 2002a). In past work, models of feedback to rhodopsin were ruled out because they produced ensemble variance that was very narrow in time, similar to receptor activity that abruptly terminates in this study. Multi-step models of gradual receptor inactivation required a large number of steps to explain the low variability of primate and guinea pig single-photon responses, on order  $\sim 12 - 14$ , and an additional model for component exhaustion could reduce this requirement.

A potential source of this regulation is the inactivating steps of phosphorylation and arrestin binding. Genetic ablation of GRK1, the substrate phosphorylation sites, or arrestin1 severely disrupt response recovery (Chen et al., 1995; Chen et al., 1999; Xu et al., 1997), while substitution of alanine for subsets of phosphorylation sites reveal a range of resulting response characteristics (Mendez et al., 2003). Prevailing experimental techniques initially prevented isolation of single-photon responses and, consequently, the characterization of their variance, but overcoming this limitation further revealed the importance of the full complement of sites in keeping the coefficient of variation of response area low (Doan et al., 2006). The sensitivity of the  $CV_{area}$  to removal of a single phosphorylation site is suggestive that variation in receptor activity translates effectively linearly to fluctuations in the outer segment membrane current. The approach presented here hypothesizes linear models for receptor and cascade but also tests the ability of two nonlinear mechanisms to mask additional receptor variability.

#### *4.5.2 Non-linear mechanisms controlling variability*

Non-linear mechanisms are recruited to expand the regime of illumination over which the rod can respond, and are critical for adaptation to light intensities above darkness (Fain et al., 2001; Koutalos and Yau, 1996). The models of mammalian phototransduction discussed thus far use a linearized version of cascade reaction equations, perhaps an oversimplification. A further simplification is to ignore the specialized rod morphology and the limitations to diffusion that it potentially creates. The extension of models to include these considerations have raised the possibility that spatial-temporal restriction of second messengers could create nonlinear relationships between cascade elements that could reduce variability in receptor activity (Andreucci et al., 2003). In particular, it appears that the tortuous geometry could prevent cGMP diffusion and enhance local depletion in the inter-disk vol-

ume by PDE hydrolysis, reducing the effectiveness of additional PDE (Caruso et al., 2011; Bisegna et al., 2008). These models indicate that cooperative channel gating and  $\text{Ca}^{2+}$  dependent feedback may also act to reduce variability, but experimental evidence suggests their effect is limited (Burns et al., 2002; Field and Rieke, 2002a).

Nevertheless, these studies emphasize the possible impact of compression, and we tested this possibility here. As predicted, increasing compression relaxes constraints on receptor inactivation, and the number of steps required to control activity can decrease as a result (Fig. 4.8. This trade-off is necessarily accompanied by a faster decay in receptor activity. However, the degree of compression that permits significant reduction in the number of inactivation steps also appears to be incompatible with increased disk activity produced by 1P and 0P mutant receptors.

Models that incorporate the geometry of the rod also suggest that these responses can be affected by changes in rod volume brought on by transgenic expression (Caruso et al., 2010). However, tandem expression of the 1P mutant receptor along with WT rhodopsin shows that even in rods which exhibit normal kinetics for wild-type responses, the mutant response amplitudes are increased, consistent with results from ectopic expression of rhodopsin mutants lacking a C-terminus (Chen et al., 1995).

#### *4.5.3 Mechanism of steps*

The multi-step shutoff model for rhodopsin inactivation presented here is attractive for its tractable implementation, its simple set of parameters, and for the general picture of desensitization kinetics it provides. Such models use the number of steps simply as a proxy for total variability: the steps are modeled as first order random processes such that the integrated activity is effectively the sum over the random, Poisson activity of each step (Rieke and Baylor, 1998a; Field and Rieke, 2002a; Doan et al., 2006). This model has been

a concise way to generate hypotheses and to drive continual investigation of mechanisms that control single-photon response kinetics, though the molecular mechanisms proposed to support this low variability have changed as hypotheses have been tested.

Phosphorylation of the receptor appears an important contributor of mechanisms reducing variability. Biochemical experiments suggest that while multiple-phosphorylation is possible (Wilden and Kühn, 1982), that not all phosphorylation sites are necessary for tight arrestin binding, or that some play more important roles than others (Kennedy et al., 2001; Maeda et al., 2003; Vishnivetskiy et al., 2007). Meanwhile, mutations of phosphorylation sites indicate both the possibility for complete phosphorylation *in vivo*, as well as the importance of the full complement of phosphorylation sites (Mendez et al., 2003; Doan et al., 2006). It is possible that different complements of sites contribute in specific ways, such that not all phosphorylation events are equivalent (Brannock et al., 1999), and particular sites may act as important structural features mediating interactions with GRK1 or arrestin1 rather than as substrates for phosphorylation (Kisselev et al., 2004). The outer-segment concentrations of arrestin1 and GRK1 also play a role, likely through competition for rhodopsin; steps could then represent the composite of multiple reactions (Doan et al., 2009).

As a more detailed picture of rhodopsin desensitization emerges, it will have to account for low ensemble variability. The approach presented here provides a framework for testing future models against experimental data.

## BIBLIOGRAPHY

- Aho AC, Donner K, Hydén C, Larsen LO, Reuter T (1988) Low retinal noise in animals with low body temperature allows high visual sensitivity. *Nature* 334:348–350.
- Ames A, Nesbett FB (1981) In vitro retina as an experimental model of the central nervous system. *Journal of Neurochemistry* 37:867–877.
- Andreucci D, Bisegna P, Caruso G, Hamm HE, Dibenedetto E (2003) Mathematical model of the spatio-temporal dynamics of second messengers in visual transduction. *Bio-physical Journal* 85:1358–1376.
- Arshavsky VY (2002) Rhodopsin phosphorylation: from terminating single photon responses to photoreceptor dark adaptation. *Trends in Neurosciences* 25:124–126.
- Arshavsky VY, Lamb TD, Pugh EN (2002) G proteins and phototransduction. *Annual Review of Physiology* 64:153–187.
- Arshavsky VY, Bownds MD (1992) Regulation of deactivation of photoreceptor G protein by its target enzyme and cGMP. *Nature* 357:416–417.
- Azevedo AW, Rieke F (2011) Experimental protocols alter phototransduction: the implications for retinal processing at visual threshold. *Journal of Neuroscience* 31:3670–3682.
- Baylor DA, Hodgkin AL (1973) Detection and resolution of visual stimuli by turtle photoreceptors. *The Journal of Physiology* 234:163–198.
- Baylor DA, Lamb TD, Yau KW (1979a) Responses of retinal rods to single photons. *The Journal of Physiology* 288:613–634.
- Baylor DA, Lamb TD, Yau KW (1979b) The membrane current of single rod outer segments. *The Journal of Physiology* 288:589–611.
- Baylor DA, Matthews G, Nunn BJ (1984) Location and function of voltage-sensitive conductances in retinal rods of the salamander, *Ambystoma tigrinum*. *The Journal of Physiology* 354:203–223.
- Baylor DA, Matthews G, Yau KW (1980) Two components of electrical dark noise in toad retinal rod outer segments. *The Journal of Physiology* 309:591–621.

- Baylor DA, Nunn BJ (1986) Electrical properties of the light-sensitive conductance of rods of the salamander *Ambystoma tigrinum*. *The Journal of Physiology* 371:115–145.
- Baylor DA, Nunn BJ, Schnapf JL (1984) The photocurrent, noise and spectral sensitivity of rods of the monkey *Macaca fascicularis*. *The Journal of Physiology* 357:575–607.
- Berntson A, Smith RG, Taylor WR (2004) Transmission of single photon signals through a binary synapse in the mammalian retina. *Visual Neuroscience* 21:693–702.
- Bialek W, Owen WG (1990) Temporal filtering in retinal bipolar cells. Elements of an optimal computation? *Biophysical Journal* 58:1227–1233.
- Bisegna P, Caruso G, Andreucci D, Shen L, Gurevich VV, Hamm HE, Dibenedetto E (2008) Diffusion of the second messengers in the cytoplasm acts as a variability suppressor of the single photon response in vertebrate phototransduction. *Biophysical Journal* 94:3363–3383.
- Brannock MT, Weng K, Robinson PR (1999) Rhodopsin's carboxyl-terminal threonines are required for wild-type arrestin-mediated quench of transducin activation in vitro. *Biochemistry* 38:3770–3777.
- Burns ME, Pugh EN (2010) Lessons from photoreceptors: turning off G-protein signaling in living cells. *Physiology* 25:72–84.
- Burns ME, Arshavsky VY (2005) Beyond counting photons: trials and trends in vertebrate visual transduction. *Neuron* 48:387–401.
- Burns ME, Mendez A, Chen J, Baylor DA (2002) Dynamics of cyclic GMP synthesis in retinal rods. *Neuron* 36:81–91.
- Burns ME, Pugh EN (2009) RGS9 concentration matters in rod phototransduction. *Biophysical Journal* 97:1538–1547.
- Calvert PD, Govardovskii VI, Krasnoperova N, Anderson RE, Lem J, Makino CL (2001) Membrane protein diffusion sets the speed of rod phototransduction. *Nature* 411:90–94.
- Calvert PD, Krasnoperova NV, Lyubarsky AL, Isayama T, Nicoló M, Kosaras B, Wong G, Gannon KS, Margolskee RF, Sidman RL, Pugh EN, Makino CL, Lem J (2000) Phototransduction in transgenic mice after targeted deletion of the rod transducin alpha-subunit. *Proceedings of the National Academy of Sciences of the United States of America* 97:13913–13918.

Caruso G, Bisegna P, Andreucci D, Lenoci L, Gurevich VV, Hamm HE, Dibenedetto E (2011) Identification of key factors that reduce the variability of the single photon response. *Proceedings of the National Academy of Sciences of the United States of America* 108:7804–7807.

Caruso G, Bisegna P, Lenoci L, Andreucci D, Gurevich VV, Hamm HE, Dibenedetto E (2010) Kinetics of rhodopsin deactivation and its role in regulating recovery and reproducibility of rod photoresponse. *PLoS Computational Biology* 6:e1001031.

Chen CK, Burns ME, He W, Wensel TG, Baylor DA, Simon MI (2000) Slowed recovery of rod photoresponse in mice lacking the GTPase accelerating protein RGS9-1. *Nature* 403:557–560.

Chen CK, Burns ME, Spencer M, Niemi GA, Chen J, Hurley JB, Baylor DA, Simon MI (1999) Abnormal photoresponses and light-induced apoptosis in rods lacking rhodopsin kinase. *Proceedings of the National Academy of Sciences of the United States of America* 96:3718–3722.

Chen CK, Woodruff ML, Chen FS, Chen D, Fain GL (2010) Background light produces a recoverin-dependent modulation of activated-rhodopsin lifetime in mouse rods. *Journal of Neuroscience* 30:1213–1220.

Chen J, Makino CL, Peachey NS, Baylor DA, Simon MI (1995) Mechanisms of rhodopsin inactivation in vivo as revealed by a COOH-terminal truncation mutant. *Science* 267:374–377.

Davenport CM, Detwiler PB, Dacey DM (2008) Effects of pH buffering on horizontal and ganglion cell light responses in primate retina: Evidence for the proton hypothesis of surround formation. *Journal of Neuroscience* 28:456–464.

DeWire SM, Ahn S, Lefkowitz RJ, Shenoy SK (2007)  $\beta$ -arrestins and cell signaling. *Annual Review of Physiology* 69:483–510.

Doan T, Azevedo AW, Hurley JB, Rieke F (2009) Arrestin competition influences the kinetics and variability of the single-photon responses of mammalian rod photoreceptors. *Journal of Neuroscience* 29:11867–11879.

Doan T, Mendez A, Detwiler PB, Chen J, Rieke F (2006) Multiple phosphorylation sites confer reproducibility of the rod's single-photon responses. *Science* 313:530–533.

Doan TA (2007) Mammalian rod's single-photon responses : what do they tell us about rapid and reliable GPCR inactivation. Ph.D. diss., University of Washington, Seattle, Washington.

- Draber S, Schultze R (1994) Detection of jumps in single-channel data containing sub-conductance levels. *Biophysical Journal* 67:1404–1413.
- Duda RO, Hart PE, Stork DG (2001) *Pattern Classification* Wiley-Interscience.
- Fahrenfort I, Steijaert M, Sjoerdsma T, Vickers E, Ripps H, Van Asselt J, Endeman D, Klooster J, Numan R, Ten Eikelder H, Von Gersdorff H, Kamermans M (2009) Hemichannel-mediated and pH-based feedback from horizontal cells to cones in the vertebrate retina. *PLoS ONE* 4:e6090.
- Fain GL, Matthews HR, Cornwall MC, Koutalos Y (2001) Adaptation in vertebrate photoreceptors. *Physiological Reviews* 81:117–151.
- Felber S, Breuer HP, Petruccione F, Honerkamp J, Hofmann KP (1996) Stochastic simulation of the transducin GTPase cycle. *Biophysical Journal* 71:3051–3063.
- Field GD, Rieke F (2002a) Mechanisms regulating variability of the single photon responses of mammalian rod photoreceptors. *Neuron* 35:733–747.
- Field GD, Rieke F (2002b) Nonlinear signal transfer from mouse rods to bipolar cells and implications for visual sensitivity. *Neuron* 34:773–785.
- Field GD, Sampath AP, Rieke F (2005) Retinal processing near absolute threshold: from behavior to mechanism. *Annual Review of Physiology* 67:491–514.
- Friedburg C, Thomas MM, Lamb TD (2001) Time course of the flash response of dark- and light-adapted human rod photoreceptors derived from the electroretinogram. *The Journal of Physiology* 534:217–242.
- Fu Y, Kefalov V, Luo DG, Xue T, Yau KW (2008) Quantal noise from human red cone pigment. *Nature Neuroscience* 11:565–571.
- Gibson SK, Parkes JH, Liebman PA (2000) Phosphorylation modulates the affinity of light-activated rhodopsin for G protein and arrestin. *Biochemistry* 39:5738–5749.
- Green DG, Kapousta-Bruneau NV (1999a) A dissection of the electroretinogram from the isolated rat retina with microelectrodes and drugs. *Visual Neuroscience* 16:727–741.
- Green DG, Kapousta-Bruneau NV (1999b) Electrophysiological properties of a new isolated rat retina preparation. *Vision Research* 39:2165–2177.
- Gross OP, Burns ME (2010) Control of rhodopsin's active lifetime by arrestin-1 expression in mammalian rods. *Journal of Neuroscience* 30:3450–3457.

Gurevich VV, Gurevich EV (2004) The molecular acrobatics of arrestin activation. *Trends in Pharmacological Sciences* 25:105–111.

Hamer RD, Nicholas SC, Tranchina D, Lamb TD, Jarvinen JLP (2005) Toward a unified model of vertebrate rod phototransduction. *Visual Neuroscience* 22:417–436.

Hamer RD, Nicholas SC, Tranchina D, Liebman PA, Lamb TD (2003) Multiple steps of phosphorylation of activated rhodopsin can account for the reproducibility of vertebrate rod single-photon responses. *The Journal of General Physiology* 122:419–444.

Hara MR, Kovacs JJ, Whalen EJ, Rajagopal S, Strachan RT, Grant W, Towers AJ, Williams B, Lam CM, Xiao K, Shenoy SK, Gregory SG, Ahn S, Duckett DR, Lefkowitz RJ (2011) A stress response pathway regulates DNA damage through  $\beta$ 2-adrenoreceptors and  $\beta$ -arrestin-1. *Nature* 477:349–353.

Hecht S, Shlaer S, Pirenne MH (1942) Energy, quanta, and vision. *The Journal of General Physiology* 25:819–840.

Herrmann R, Lobanova ES, Hammond T, Kessler C, Burns ME, Frishman LJ, Arshavsky VY (2010) Phosducin regulates transmission at the photoreceptor-to-ON-bipolar cell synapse. *Journal of Neuroscience* 30:3239–3253.

Hetling JR, Pepperberg DR (1999) Sensitivity and kinetics of mouse rod flash responses determined in vivo from paired-flash electroretinograms. *The Journal of Physiology* 516 ( Pt 2):593–609.

Hirasawa H, Kaneko A (2003) pH changes in the invaginating synaptic cleft mediate feedback from horizontal cells to cone photoreceptors by modulating Ca<sup>2+</sup> channels. *The Journal of General Physiology* 122:657–671.

Kennedy MJ, Lee KA, Niemi GA, Craven KB, Garwin GG, Saari JC, Hurley JB (2001) Multiple phosphorylation of rhodopsin and the in vivo chemistry underlying rod photoreceptor dark adaptation. *Neuron* 31:87–101.

Kisselev OG, Downs MA, McDowell JH, Hargrave PA (2004) Conformational changes in the phosphorylated C-terminal domain of rhodopsin during rhodopsin arrestin interactions. *The Journal of Biological Chemistry* 279:51203–51207.

Koutalos Y, Yau KW (1996) Regulation of sensitivity in vertebrate rod photoreceptors by calcium. *Trends in Neurosciences* 19:73–81.

Krispel CM, Chen D, Melling N, Chen YJ, Martemyanov KA, Quillinan N, Arshavsky VY, Wensel TG, Chen CK, Burns ME (2006) RGS expression rate-limits recovery of rod photoresponses. *Neuron* 51:409–416.

- Laitko U, Hofmann KP (1998) A model for the recovery kinetics of rod phototransduction, based on the enzymatic deactivation of rhodopsin. *Biophysical Journal* 74:803–815.
- Lamb TD (1994) Stochastic simulation of activation in the G-protein cascade of phototransduction. *Biophysical Journal* 67:1439–1454.
- Lamb TD, Pugh EN (1992) A quantitative account of the activation steps involved in phototransduction in amphibian photoreceptors. *The Journal of Physiology* 449:719–758.
- Lefkowitz RJ (2007) Seven transmembrane receptors: something old, something new. *Acta Physiologica (Oxford, England)* 190:9–19.
- Liang Y, Fotiadis D, Maeda T, Maeda A, Modzelewska A, Filipek S, Saperstein DA, Engel A, Palczewski K (2004) Rhodopsin signaling and organization in heterozygote rhodopsin knockout mice. *The Journal of Biological Chemistry* 279:48189–48196.
- Luo DG, Yau KW (2005) Rod sensitivity of neonatal mouse and rat. *The Journal of General Physiology* 126:263–269.
- Lyubarsky AL, Pugh EN (1996) Recovery phase of the murine rod photoresponse reconstructed from electroretinographic recordings. *The Journal of Neuroscience* 16:563–571.
- Maeda T, Imanishi Y, Palczewski K (2003) Rhodopsin phosphorylation: 30 years later. *Progress in Retinal and Eye Research* 22:417–434.
- Makino CL, Dodd RL, Chen J, Burns ME, Roca A, Simon MI, Baylor DA (2004) Recoverin regulates light-dependent phosphodiesterase activity in retinal rods. *The Journal of General Physiology* 123:729–741.
- Mendez A, Burns ME, Roca A, Lem J, Wu LW, Simon MI, Baylor DA, Chen J (2000) Rapid and reproducible deactivation of rhodopsin requires multiple phosphorylation sites. *Neuron* 28:153–164.
- Mendez A, Burns ME, Sokal I, Dizhoor AM, Baehr W, Palczewski K, Baylor DA, Chen J (2001) Role of guanylate cyclase-activating proteins (GCAPs) in setting the flash sensitivity of rod photoreceptors. *Proceedings of the National Academy of Sciences of the United States of America* 98:9948–9953.
- Mendez A, Lem J, Simon M, Chen J (2003) Light-dependent translocation of arrestin in the absence of rhodopsin phosphorylation and transducin signaling. *Journal of Neuroscience* 23:3124–3129.
- Mulgrew AC (2011) A geometric approach to study the relationship between maternal and fetal characteristics and the shape of placental surfaces Technical report, Department of Mathematics and Statistics California State University, Long Beach.

Naarendorp F, Esdaille TM, Banden SM, Andrews-Labenski J, Gross OP, Pugh EN (2010) Dark light, rod saturation, and the absolute and incremental sensitivity of mouse cone vision. *Journal of Neuroscience* 30:12495–12507.

Nagy A (2003) *Manipulating the Mouse Embryo: A Laboratory Manual*. Cold Spring Harbor Laboratory Press.

Nikonov S, Engheta N, Pugh EN (1998) Kinetics of recovery of the dark-adapted salamander rod photoresponse. *The Journal of General Physiology* 111:7–37.

Nikonov S, Lamb TD, Pugh EN (2000) The role of steady phosphodiesterase activity in the kinetics and sensitivity of the light-adapted salamander rod photoresponse. *The Journal of General Physiology* 116:795–824.

Nobles KN, Xiao K, Ahn S, Shukla AK, Lam CM, Rajagopal S, Strachan RT, Huang TY, Bressler EA, Hara MR, Shenoy SK, Gygi SP, Lefkowitz RJ (2011) Distinct phosphorylation sites on the  $\beta$ 2-adrenergic receptor establish a barcode that encodes differential functions of  $\beta$ -arrestin. *Science Signaling* 4:ra51.

Oakley RH (2000) Differential affinities of visual arrestin, beta arrestin1, and beta arrestin2 for g protein-coupled receptors delineate two major classes of receptors. *Journal of Biological Chemistry* 275:17201–17210.

Ohguro H, Johnson RS, Ericsson LH, Walsh KA, Palczewski K (1994) Control of rhodopsin multiple phosphorylation. *Biochemistry* 33:1023–1028.

Ohguro H, Palczewski K, Ericsson LH, Walsh KA, Johnson RS (1993) Sequential phosphorylation of rhodopsin at multiple sites. *Biochemistry* 32:5718–5724.

Ohguro H, Van Hooser JP, Milam AH, Palczewski K (1995) Rhodopsin phosphorylation and dephosphorylation in vivo. *The Journal of Biological Chemistry* 270:14259–14262.

Okawa H, Miyagishima KJ, Arman AC, Hurley JB, Field GD, Sampath AP (2010) Optimal processing of photoreceptor signals is required to maximize behavioural sensitivity. *The Journal of Physiology* 588:1947–1960.

Pepperberg DR, Birch DG, Hood DC (1997) Photoresponses of human rods *in vivo* derived from paired-flash electroretinograms. *Visual Neuroscience* 14:73–82.

Pepperberg DR, Cornwall MC, Kahlert M, Hofmann KP, Jin J, Jones GJ, Ripps H (1992) Light-dependent delay in the falling phase of the retinal rod photoresponse. *Visual Neuroscience* 8:9–18.

- Peshenko IV, Olshevskaya EV, Dizhoor AM (2008) Binding of guanylyl cyclase activating protein 1 (GCAP1) to retinal guanylyl cyclase (RetGC1): the role of individual ef-hands. *Journal of Biological Chemistry* 283:21747–21757.
- Pugh EN, Lamb TD (1993) Amplification and kinetics of the activation steps in photo-transduction. *Biochimica et Biophysica Acta* 1141:111–149.
- Rao-Mirotznik R, Harkins AB, Buchsbaum G, Sterling P (1995) Mammalian rod terminal: architecture of a binary synapse. *Neuron* 14:561–569.
- Reiter E, Lefkowitz RJ (2006) GRKs and  $\beta$ -arrestins: roles in receptor silencing, trafficking and signaling. *Trends in Endocrinology & Metabolism* 17:159–165.
- Rieke F, Baylor DA (1996) Molecular origin of continuous dark noise in rod photoreceptors. *Biophysical Journal* 71:2553–2572.
- Rieke F, Baylor DA (1998a) Origin of reproducibility in the responses of retinal rods to single photons. *Biophysical Journal* 75:1836–1857.
- Rieke F, Baylor D (1998b) Single-photon detection by rod cells of the retina. *Reviews of Modern Physics* 70:1027–1036.
- Robson JG, Maeda H, Saszik SM, Frishman LJ (2004) In vivo studies of signaling in rod pathways of the mouse using the electroretinogram. *Vision Research* 44:3253–3268.
- Rodieck RW (1998) *The First Steps in Seeing*. Sinauer Associates Inc.
- Sakitt B (1972) Counting every quantum. *The Journal of Physiology* 223:131–150.
- Sampath AP, Rieke F (2004) Selective transmission of single photon responses by saturation at the rod-to-rod bipolar synapse. *Neuron* 41:431–443.
- Sampath AP, Strissel KJ, Elias R, Arshavsky VY, McGinnis JF, Chen J, Kawamura S, Rieke F, Hurley JB (2005) Recoverin improves rod-mediated vision by enhancing signal transmission in the mouse retina. *Neuron* 46:413–420.
- Saszik SM, Robson JG, Frishman LJ (2002) The scotopic threshold response of the dark-adapted electroretinogram of the mouse. *The Journal of Physiology* 543:899–916.
- Schein S, Ahmad KM (2005) A clockwork hypothesis: synaptic release by rod photoreceptors must be regular. *Biophysical Journal* 89:3931–3949.
- Schein S, Ahmad KM (2006) Efficiency of synaptic transmission of single-photon events from rod photoreceptor to rod bipolar dendrite. *Biophysical Journal* 91:3257–3267.

Schnapf JL, Nunn BJ, Meister M, Baylor DA (1990) Visual transduction in cones of the monkey, *Macaca fascicularis*. *The Journal of Physiology* 427:681–713.

Sharpe L, Stockman I (2000) Rod pathways: the importance of seeing nothing. *Trends in Neurosciences* 23:39.

Song X, Vishnivetskiy SA, Gross OP, Emelianoff K, Mendez A, Chen J, Gurevich EV, Burns ME, Gurevich VV (2009) Enhanced arrestin facilitates recovery and protects rods lacking rhodopsin phosphorylation. *Current Biology* 19:700–705.

Teller DC, Okada T, Behnke CA, Palczewski K, Stenkamp RE (2001) Advances in determination of a high-resolution three-dimensional structure of rhodopsin, a model of G-protein-coupled receptors (GPCRs). *Biochemistry* 40:7761–7772.

Tobin AB, Butcher AJ, Kong KC (2008) Location, location, location...site-specific GPCR phosphorylation offers a mechanism for cell-type-specific signalling. *Trends in pharmacological sciences* 29:413–420.

van Rossum MC, Smith RG (1998) Noise removal at the rod synapse of mammalian retina. *Visual Neuroscience* 15:809–821.

Violin JD, Ren XR, Lefkowitz RJ (2006) G-protein-coupled receptor kinase specificity for beta-arrestin recruitment to the beta<sub>2</sub>-adrenergic receptor revealed by fluorescence resonance energy transfer. *The Journal of Biological Chemistry* 281:20577–20588.

Vishnivetskiy SA, Raman D, Wei J, Kennedy MJ, Hurley JB, Gurevich VV (2007) Regulation of arrestin binding by rhodopsin phosphorylation level. *Journal of Biological Chemistry* 282:32075–32083.

Wen XH, Shen L, Brush RS, Michaud N, Al-Ubaidi MR, Gurevich VV, Hamm HE, Lem J, Dibenedetto E, Anderson RE, Makino CL (2009) Overexpression of rhodopsin alters the structure and photoresponse of rod photoreceptors. *Biophysical Journal* 96:939–950.

Wensel TG (2008) Signal transducing membrane complexes of photoreceptor outer segments. *Vision Research* 48:2052–2061.

Whitlock GG, Lamb TD (1999) Variability in the time course of single photon responses from toad rods: termination of rhodopsin's activity. *Neuron* 23:337–351.

Wilden U, Kühn H (1982) Light-dependent phosphorylation of rhodopsin: number of phosphorylation sites. *Biochemistry* 21:3014–3022.

Winkler BS, Simson V, Benner J (1977) Importance of bicarbonate in retinal function. *Investigative Ophthalmology & Visual Science* 16:766–768.

Xu J, Dodd RL, Makino CL, Simon MI, Baylor DA, Chen J (1997) Prolonged photore-sponses in transgenic mouse rods lacking arrestin. *Nature* 389:505–509.

Yau KW, Lamb TD, Baylor DA (1977) Light-induced fluctuations in membrane current of single toad rod outer segments. *Nature* 269:78–80.